Validation of the Mann spectral tensor for offshore wind conditions at different atmospheric stabilities

de Mare, Martin Tobias; Mann, Jakob

Published in:
Journal of Physics: Conference Series (Online)

Link to article, DOI:
10.1088/1742-6596/524/1/012106

Publication date:
2014

Document Version
Publisher's PDF, also known as Version of record

Validation of the Mann spectral tensor for offshore wind conditions at different atmospheric stabilities

2014 J. Phys.: Conf. Ser. 524 012106

(http://iopscience.iop.org/1742-6596/524/1/012106)

Validation of the Mann spectral tensor for offshore wind conditions at different atmospheric stabilities

Martin de Maré[1,2] **and Jakob Mann**[2]

[1] DONG Energy A/S, Denmark
[2] Wind Energy Department, Risø DTU, Denmark

E-mail: mardm@dongenergy.dk

Abstract. Simulated wind fields are very useful when predicting loads on structures subjected to turbulent winds, wind turbines being a prime example. Knowledge of statistical properties such as the spatial and temporal correlations of real turbulent wind fields increases the realism of the simulated simulated wind fields. The statistical properties of real turbulent wind fields have been shown to depend on quantities such as the surface roughness, the mean wind speed, measurement height and atmospheric stability. The Mann spectral tensor attempts to predict all spatial correlations of shear generated turbulence given only three input parameters. The most suitable such input values have been investigated for different onshore surface roughnesses, but so far not for typical offshore conditions. The meteorological mast at the Rødsand II offshore wind farm has among other instruments sonic anemometers mounted at 15, 40 and 57 meters above sea level. Wind speed spectra at the three heights are calculated and binned with respect to both wind speed and atmospheric stability. The three parameters of the Mann spectral tensor are determined to ensure best fit to the spectra of each of the bins and are presented as a function of mean wind speed, measurement height and atmospheric stability. The behaviour of the presented parameters values are largely consistent with the previous onshore results. The parameter values are also compared to potentially related quantities and a constant quantity is derived. Given optimal parameters the spectral tensor is found to reproduce the surface layer generated turbulence well, also for different atmospheric stabilities, however in the wind speed spectra a contribution from the very large scale quasi-geostrophic turbulence is also observed, a contribution the spectral tensor does not attempt to model.

1. Introduction

The Mann spectral tensor [3] attempts to predict all second order spatial statistics of shear generated turbulence given only three input parameters, $\alpha\epsilon^{2/3}$, L_M and Γ. The tensor can for example be used to generate realistic simulated turbulent wind fields, see [4]. These simulated wind fields are very useful as input to aero-elastic simulation of structures subjected to turbulent flows, wind turbines being a prime example.

The statistical properties of real turbulent wind fields has been shown to depend on quantities such as the surface roughness, the mean wind speed, measurement height and atmospheric stability. Although the Mann spectral tensor is developed for neutral atmospheric stability, the parameter values which describe the turbulence best for different atmospheric stabilities has been investigated using onshore measurements, see e.g. [1] and [6]. We will attempt to determine the

parameter values suitable for offshore conditions, at different wind speed, measurement height and atmospheric stability.

2. Methodology

The data was collected at the meteorological mast at the Rødsand II offshore wind farm, which is situated just south of the Danish island Lolland, from February 2010 to October 2012. We select wind directions from 255° to 285° where the wind has a fetch over water of approximately 100km. Among other instruments the mast has 3 Campbell Scientific sonic anemometers, a type that includes a temperature sensor, at 15, 40 and 57 meters above sea level. We will quantify atmospheric stability based on the Monin-Obukhov length [5], which is defined as

$$L = -\frac{{u_{*0}}^3 T_0}{\kappa g \overline{u_3 \Theta'_{v0}}} \tag{1}$$

where $u_{*0} = \sqrt{-\overline{u_1 u_3}}$ is the friction velocity, T_0 is the absolute temperature, $\kappa \approx 0.4$ is the von Karman constant and Θ'_v is the fluctuation in virtual potential temperature, all at the surface. We approximate these surface values with values measured at 15 m.

We employ Taylor's frozen turbulence assumption in order to estimate the spatial cross-spectra defined as

$$F_{ij}\left(k_1\right) = \frac{1}{2\pi} \int \left\langle u_i(\boldsymbol{x}, t)\, u_j(\boldsymbol{x} + (r_1, 0, 0)\,, t) \right\rangle e^{-\mathrm{i} k_1 r_1} \mathrm{d}r_1 \tag{2}$$

from 30-minute periods of measured wind velocities. These calculated cross-spectra are compared to cross-spectra derived from the spectral tensor, see [3].

We bin the data simultaneously for the 3 atmospheric stability classes shown in in table 1 and 3 wind speed bins, 8, 10 and 12 $\mathrm{ms}^{-1} \pm 1\ \mathrm{ms}^{-1}$, based on the anemometer at 15 m, resulting in a total of 9 bins per measurement height.

Table 1: Atmospheric stability bins

Atmospheric stability class	Monin-Obukhov length interval (m)
Unstable (U)	$-200 \leq L \leq -100$
Neutral (N)	$500 \leq \lvert L \rvert$
Stable (S)	$50 \leq L \leq 200$

In each bin the spectra are normalized with the for each time period corresponding u_{*0}. The normalized spectra are averaged using the method of bins with respect to $\log(k_1)$, using a bin size of $0.2 \log(10)$. In order to make the fitting algorithm more robust we depart from the fitting procedure outlined in [3] in that we first determine L_M by fitting all parameters only to $F_{33}\left(k_1\right)$ and $F_{13}\left(k_1\right)$. Keeping L_M constant we then use $F_{11}\left(k_1\right)$, $F_{22}\left(k_1\right)$ and $F_{33}\left(k_1\right)$ to determine which $\alpha\epsilon^{2/3}$ and Γ that gives the best fit. In this last step we only use one decade of the spectra, centered around $k_1 = L_M^{-1}$. For bins where both algorithms performed well, no systematic change in the resulting parameter values due to the change in method was observed.

The vertical wind speed gradient, $\frac{\partial U}{\partial z}$, is calculated by fitting a logarithmic profile to the mean wind speeds at the 3 measurement heights. This method is robust but not very precise as the

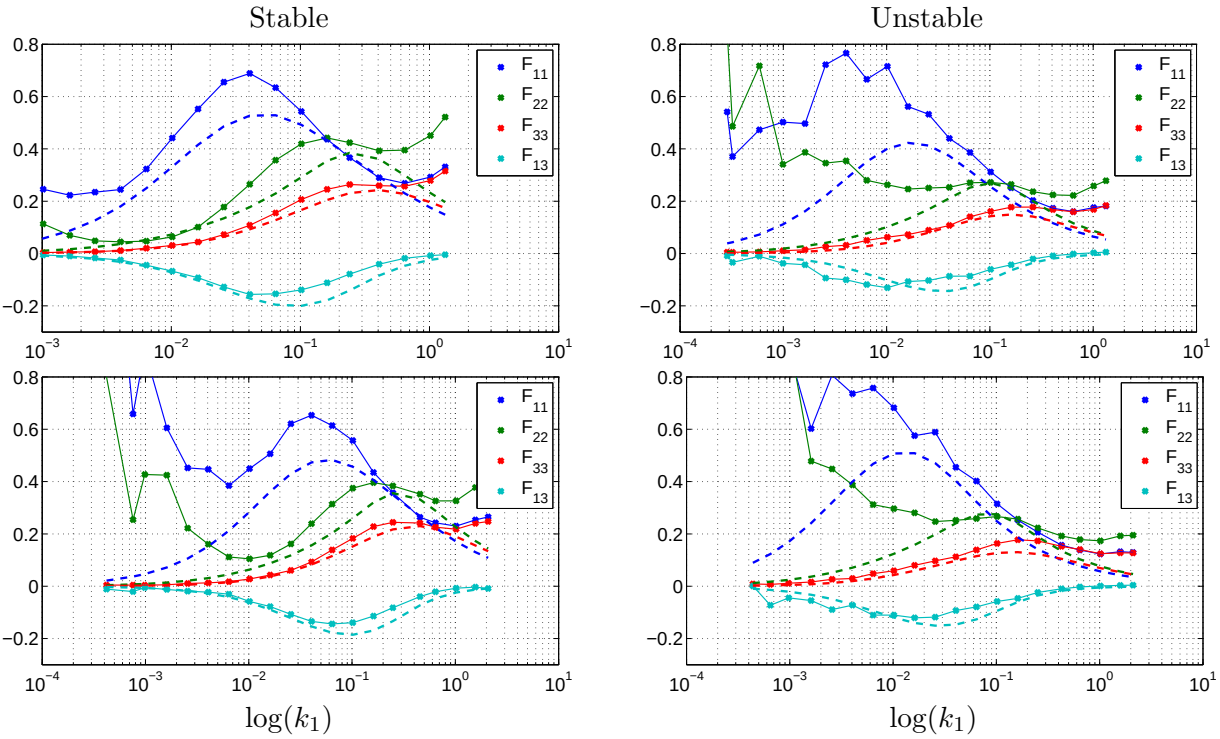

Figure 1: Spectra, $k_1E(k_1)/{u_{*0}}^2$ versus $\log(k_1)$ for the bins Stable and Unstable at 15 meters. The top row graphs shows spectra from the wind speed bin 12 ms^{-1} and bottom row show the wind speed bin 8 ms^{-1}. The broken lines are the best fit of spectra derived from the Mann spectral tensor. For the F_{11} and F_{22} components we notice high energy levels at low wave numbers which are not matched in the Mann spectral tensor spectra, especially for the lower wind speed bin (bottom row).

wind profile is expected to be logarithmic only for the neutral case and then only close to the ground where u_* is approximately constant. We see in the graph to the right in figure 7 that assuming u_* to be constant is a not a good approximation in this case.

3. Results and discussion

The performance of the fitting algorithm is exemplified in figure 1 where the calculated spectra from a few bins are shown. We notice relatively high energy levels at low wave numbers which are not matched in the Mann spectral tensor spectra, especially in the lower wind speed bin. This behavior is not present in the vertical (red) component, which suggests that we are observing the high wave number end of the very large scale *quasi-geostrophic* turbulence, discussed e.g. in [2] and [8]. In figure 2 spectra using 90 minutes instead of 30 minutes of data are shown for the bins Stable and Unstable at 15 meters. The streamwise and lateral component shows a $|\boldsymbol{k}|^{-5/3}$-slope for low wave numbers, which is consistent with this being quasi-geostrophic turbulence.

In figures in 3 to 5 the resulting parameter values are plotted as a function of measurement height and wind speed. We notice that the wind speed has almost no influence on the parameter values while both atmospheric stability and measurement height are important factors. The results in figures 3 to 5 are consistent with what was observed in [1] and [6] except for the value of the parameter Γ which here and in [1] decreases with stability, while [6] reports a more complex behavior.

Studying the equation for turbulent kinetic energy which can be derived from the Navier-Stokes

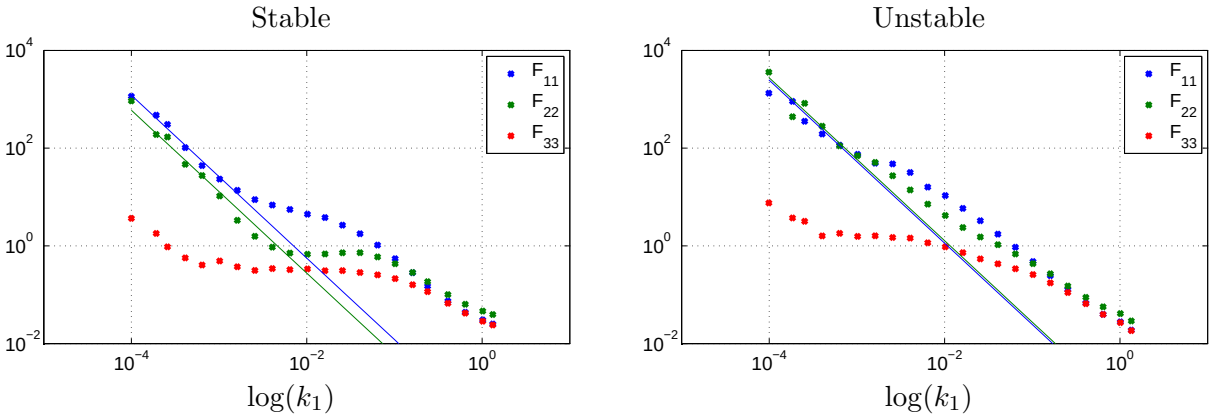

Figure 2: Spectra using 90 minutes of data, $\log(E(k_1))$ versus $\log(k_1)$, for the bins Stable and Unstable at 15 meters. The solid lines highlight the $|\boldsymbol{k}|^{-5/3}$-slope of $E(k_1)$ for low wave numbers. The fact that the wind speed bin is 12 ms^{-1} shows that this contribution is present also for high wind speeds.

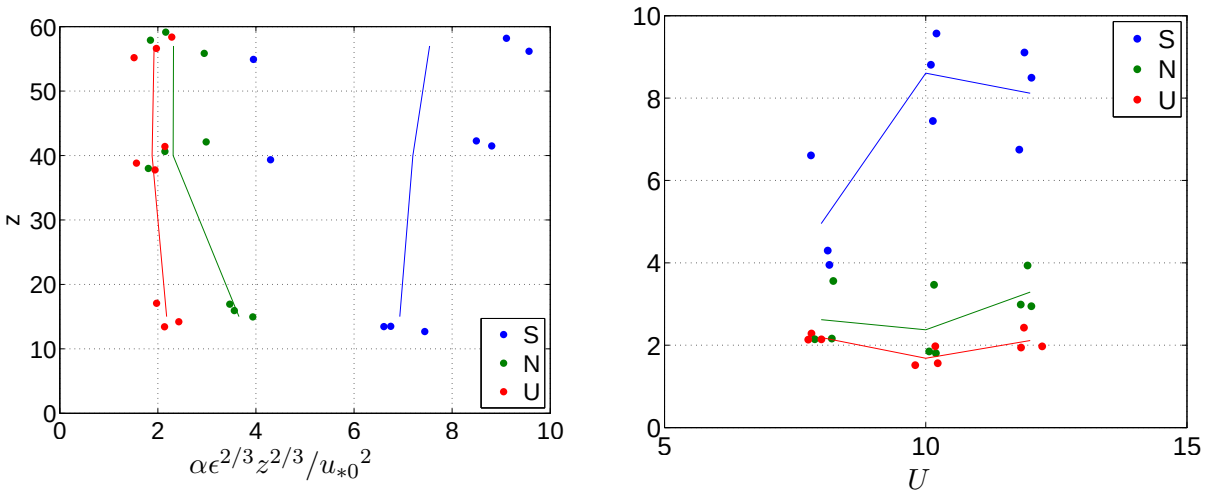

Figure 3: The parameter $\alpha\epsilon^{2/3}$ normalized with measurement height z and u_{*0} as a function of measurement height and wind speed U. A small random offset has been added to the measurement height and wind speed for readability. Note that the x-axis of the left plot is the y-axis of the right plot.

equation the energy transfer from the mean flow is $-\overline{u_1 u_3}\frac{\partial U}{\partial z}$. In the left plot of figure 6 we see this turbulent energy production to the power $\frac{2}{3}$ divided by $\alpha\epsilon^{2/3}$. If the production and the dissipation were in perfect balance we would expect this ratio to be $\frac{1}{\alpha}$. In [7] the value 0.5 of C_k, the Kolmogorov constant for the one-dimensional spectra, is proposed, and this value combined with $\alpha = \frac{55}{18}C_k$ gives $\frac{1}{\alpha} \approx 0.65$.

In the plot to the right in figure 6 we see the ratio between the mixing length defined by $l_{mix}\frac{\partial U}{\partial z} = u_*$, and L_M. The result agrees reasonably but not perfectly with the $\frac{1}{1.70} \approx 0.59$ reported in [6].

In [3] the so called eddy life time, $\tau(|\boldsymbol{k}|)$, is given by

$$\tau(|\boldsymbol{k}|) = \Gamma \left(\frac{\partial U}{\partial z}\right)^{-1} \frac{|\boldsymbol{k}|^{-2/3} L_M^{-2/3}}{\sqrt{{}_2\mathrm{F}_1\left(\frac{1}{3}, \frac{17}{6}, \frac{4}{3}, -|\boldsymbol{k}|^{-2} L_M^{-2}\right)}}. \tag{3}$$

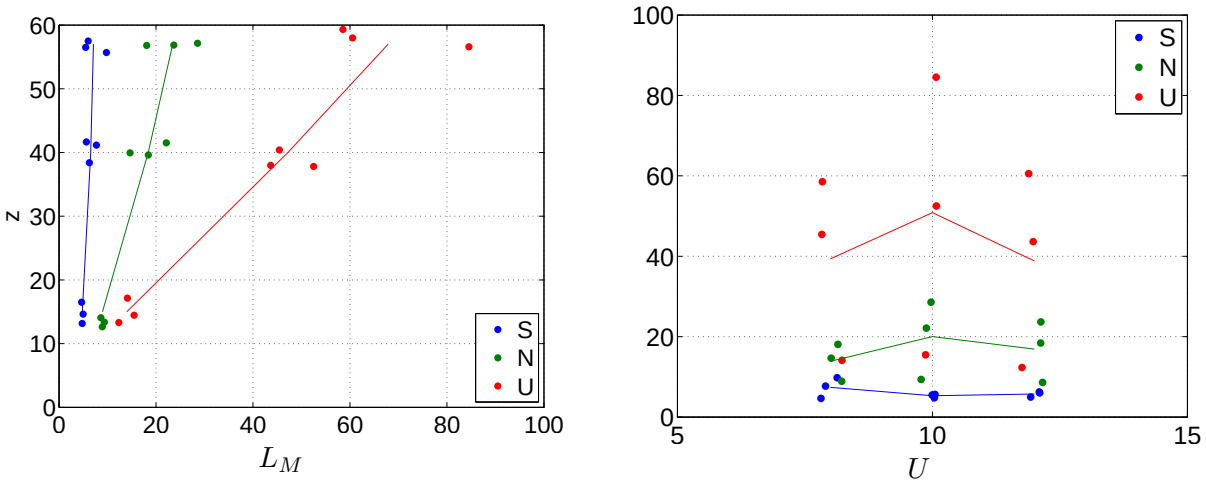

Figure 4: The parameter L_M as a function of measurement height z and wind speed U. A small random offset has been added to the measurement height and wind speed for readability. Note that the x-axis of the left plot is the y-axis of the right plot.

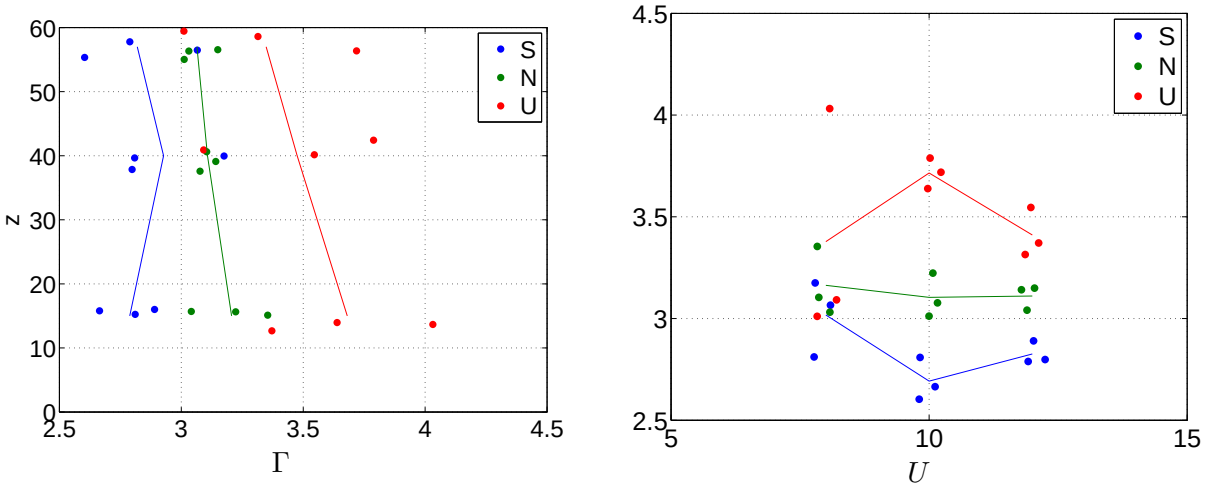

Figure 5: The parameter Γ as a function of measurement height z and wind speed U. A small random offset has been added to the measurement height and wind speed for readability. Note that the x-axis of the left plot is the y-axis of the right plot.

For $|\boldsymbol{k}|\, L_M \gg 1$ the hypergeometric function ${}_2\mathrm{F}_1\left(\frac{1}{3}, \frac{17}{6}, \frac{4}{3}, -|\boldsymbol{k}|^{-2} L_M^{-2}\right) \approx 1$. Thus for a $\boldsymbol{k}$ in the inertial subrange

$$\tau(|\boldsymbol{k}|) \approx \Gamma \left(\frac{\partial U}{\partial z}\right)^{-1} |\boldsymbol{k}|^{-2/3} L_M^{-2/3}. \tag{4}$$

Alternatively we can argue that, in the inertial subrange, τ should only be a function of $|\boldsymbol{k}|$ and the energy dissipation, ϵ, which using dimensional analysis leads to

$$\tau(|\boldsymbol{k}|) \propto |\boldsymbol{k}|^{-2/3} \epsilon^{-1/3}. \tag{5}$$

Eliminating $\tau(|\boldsymbol{k}|)$ by combining (4) and (5) leads us to the conclusion that $\frac{\Gamma \epsilon^{1/3}}{\frac{\partial U}{\partial z}\, L_M^{2/3}}$ should be

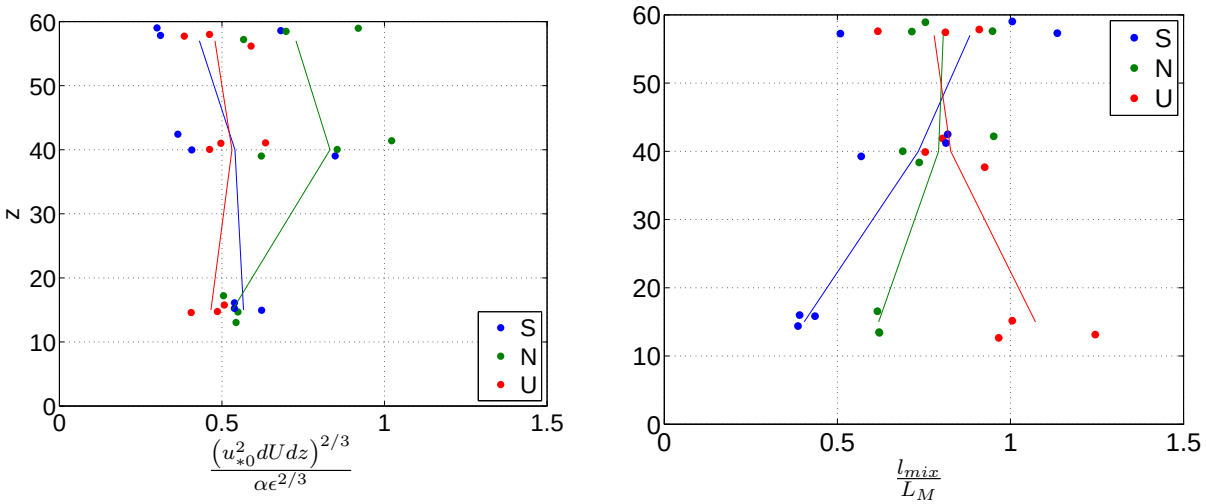

Figure 6: To the left, the quantity $\frac{\left(u_{*0}^2 \frac{\partial U}{\partial z}\right)^{2/3}}{\alpha\epsilon^{2/3}}$ which we expect to be approximately equal to $\frac{1}{\alpha} \approx 0.65$ versus measurement height. To the right the ratio $\frac{l_{mix}}{L_M}$ versus measurement height agrees reasonably but not perfectly with the $\frac{1}{1.70} \approx 0.59$ presented in [6]. A small random offset has been added to the measurement height.

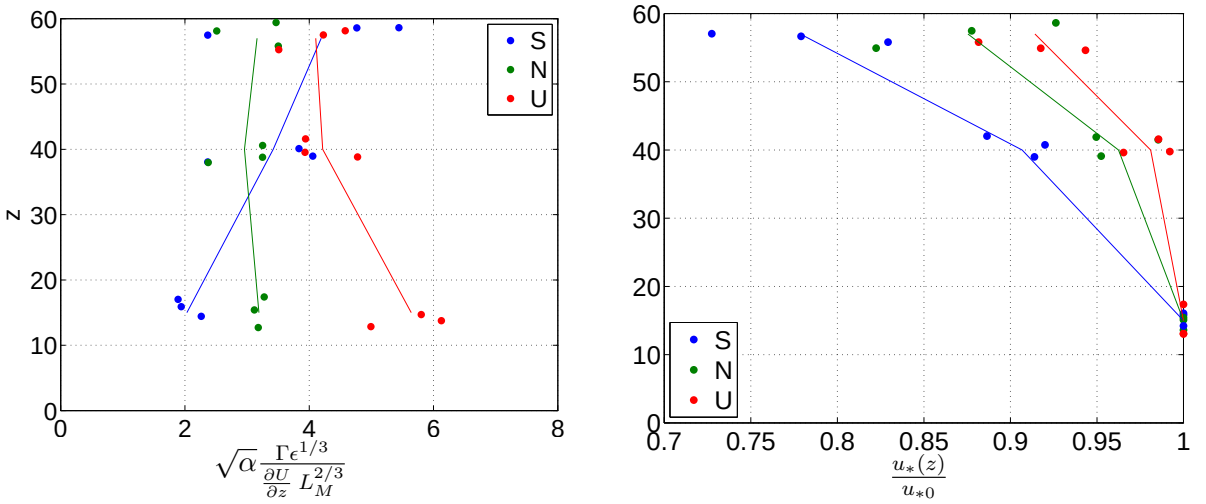

Figure 7: To the left the quantity $\sqrt{\alpha}\frac{\Gamma\epsilon^{1/3}}{\frac{\partial U}{\partial z} L_M^{2/3}}$, which we expect to be constant, plotted versus measurement height. If we focus exclusively on the Neutral case (green) then $\sqrt{\alpha}\frac{\Gamma\epsilon^{1/3}}{\frac{\partial U}{\partial z} L_M^{2/3}} \approx 3$. In the graph to the right $\frac{u_*(z)}{u_{*0}}$ versus measurement height illustrates that we are not generally measuring in the surface layer, as if so u_* would be approximately constant. A small random offset has been added to the measurement height.

constant. In the left graph of figure 7 the quantity $\sqrt{\alpha}\frac{\Gamma\epsilon^{1/3}}{\frac{\partial U}{\partial z} L_M^{2/3}}$ is plotted versus measurement height. There is a lot of scatter in the graph but if we should assign a value we recommend $\sqrt{\alpha}\frac{\Gamma\epsilon^{1/3}}{\frac{\partial U}{\partial z} L_M^{2/3}} \approx 3$ as the neutral data is likely most reliable due to the method used to derive $\frac{\partial U}{\partial z}$. The graph to the right in figure 7 illustrates that we are not generally measuring in the surface

layer, and this could explain some of the scatter in figures 6 and 7 as they show results derived using $\frac{\partial U}{\partial z}$ which, as mentioned is calculated using a methodology suitable to the surface layer.

4. Conclusions

The parameter values giving the best fit of spectra calculated from the Mann spectral tensor to measured spectra was observed using data from the offshore meteorological mast at Rødsand II. Given optimal parameters the spectral tensor reproduces 3-dimensional turbulence contribution well, also for different atmospheric stabilities.

The results are consistent with what was observed in [1] and [6] except for the value of the parameter Γ which here and in [1] decreases with stability, while [6] reports a more complex behavior.

It was argued that the quantity $\sqrt{\alpha}\frac{\Gamma\epsilon^{1/3}}{\frac{\partial U}{\partial z}L_M^{2/3}}$ should be constant and the value ≈ 3 for was proposed for this constant.

At the low wavenumber end of the spectra a contribution from quasi-geostrophic turbulence was observed.

References

[1] Abhijit S Chougule. *Influence of atmospheric stability on the spatial structure of turbulence*. DTU Wind Energy PhD-0028 (EN), 2013.
[2] Erik Lindborg. Can the atmospheric kinetic energy spectrum be explained by two-dimensional turbulence? *Journal of Fluid Mechanics*, 388:259–288, June 1999.
[3] Jakob Mann. The spatial structure of neutral atmospheric surface-layer turbulence. *Journal of Fluid Mechanics*, 273:141–168, April 1994.
[4] Jakob Mann. Wind field simulation. *Probabilistic Engineering Mechanics*, 13(4):269–282, October 1998.
[5] Andrei S Monin and Alexander M Obukhov. Basic laws of turbulent mixing in the surface layer of the atmosphere. 24(151):163–187, 1959.
[6] Alfredo Peña, Sven-Erik Gryning, and Jakob Mann. On the length-scale of the wind profile. *Quarterly Journal of the Royal Meteorological Society*, 136(653):2119–2131, October 2010.
[7] Katepalli R Sreenivasan. On the universality of the Kolmogorov constant. *Physics of Fluids (1994-present)*, 7(11), 1995.
[8] Ka Kit Tung, Wendell W Orlando, and Tyler Welch. On the differences between 2D and QG turbulence. *Discrete and continous dynamical systems - Series B*, 3(2):145–162, 2003.